Beamwidth Effects on the Differential Phase Measurements of Rain

ALEXANDER RYZHKOV

Cooperative Institute for Mesoscale Meteorological Studies (CIMMS), University of Oklahoma, Norman, Oklahoma

DUSAN ZRNIC

National Severe Storms Laboratory, Norman, Oklahoma

(Manuscript received 14 January 1997, in final form 22 July 1997)

ABSTRACT

Effects of beamfilling nonuniformities on the differential phase and rainfall estimation that use specific differential phase are examined. Two physical models are considered: an isolated rain cell with azimuthal dimensions comparable to the beamwidth and a sharp rain boundary approximating a squall line. The model results are compared to observations. An extension of the analysis to include observations of the melting layer is made. From this analysis emerges an interpretation of the radial profile of differential phase that varies from previous explanations. The current interpretation might be favored due to its simplicity and reliance on accepted physical properties of the melting layer.

1. Introduction

The polarimetric technique for rainfall estimation based on the specific differential phase measurements has important advantages compared to routine methods that use *Z–R* relations (Zrnic and Ryzhkov 1996). In contrast to the reflectivity factor *Z*, the specific differential phase K_{DP} is immune to radar calibration errors, attenuation in precipitation, and radar beam blockage, and is less susceptible to drop size distribution variations and presence of hail (Zrnic and Ryzhkov 1996). Recent analysis of rain accumulations over a test area located between 50 and 80 km from the National Severe Storms Laboratory's (NSSL) Cimarron polarimetric radar indicates superior performance of the differential phase algorithm at distances close to the radar where range effects such as beam broadening and height above the ground are not overwhelming (Ryzhkov and Zrnic 1996).

However, it was observed that at greater distances, the contours of rain cells derived from *Z* and K_{DP} measurements can differ. Moreover, areas with negative K_{DP} sometimes appear in regions of pronounced azimuthal gradients of *Z*, most frequently at the rear sides of isolated convective cells or near the leading edges of squall lines. Because of the large magnitude of these negative excursions and ''coherent appearance'' these negative K_{DP} signatures cannot be attributed to statistical fluctuations of the estimates. Neither are they caused by vertically oriented crystals, such as routinely observed in the upper portions of thunderstorms (Caylor and Chandrasekar 1996), nor by backscatter differential phase that can be expected in the presence of large hail (Zrnic et al. 1993a).

Ryzhkov and Zrnic (1996) attribute these negative K_{DP} signatures to large azimuthal gradients within the radar resolution volume. Sharp changes in the reflectivity factor within the resolution volume are more likely at larger distances from the radar, therefore the probability of occurrence of negative K_{DP}'s increases with increasing range from the radar. We point out (Zrnic and Ryzhkov 1996) that the apparent boundaries of rain cells (at great distances) estimated from K_{DP} can differ from those inferred from *Z*. The K_{DP} images of rain cells are wider in the azimuthal direction than the *Z* images.

This paper provides a more detailed analysis of the effect of beamfilling nonuniformity on the differential phase and rainfall estimates. We simulate the total differential phase Φ_{DP}, the specific differential phase K_{DP}, as well as the rain-rate fields $R(K_{DP})$ and $R(Z)$ derived from K_{DP} and *Z*. Two simple models are examined: an isolated rain cell with the azimuthal size comparable to that of the radar beam and a line of sharp reflectivity change seen at an angle from the radar. The latter approximates a squall line. We also model the melting layer and associated bright band with a sharp discontinuity in the vertical plane. Theoretical conclusions are supported by experimental data collected with the NSSL's polarimetric radar in Oklahoma and with the NCAR's polarimetric radar in Colorado; both radars have a wavelength of 10 cm.

Corresponding author address: Dr. Alexander V. Ryzhkov, NSSL/CIMMS, 1313 Halley Circle, Norman, OK 73069.
E-mail: ryzhkov@nsslsun.nssl.uoknor.edu

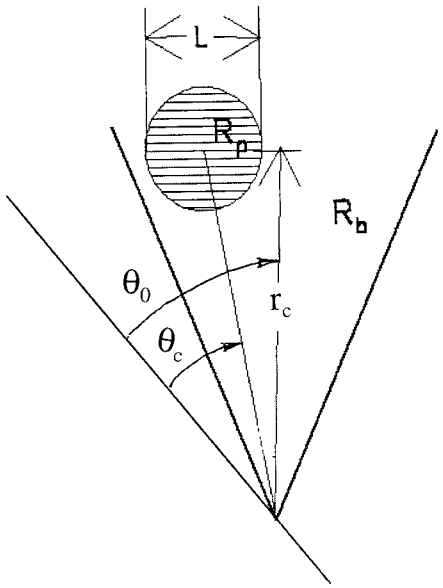

FIG. 1. Conceptual model of an isolated rain cell; R_p is a peak rain rate in the cell and R_b is a background rain rate.

2. Isolated rain cell

The model of an isolated rain cell is illustrated in Fig. 1. It assumes that the rain cell, with peak rain rate R_p, is immersed in a uniform background rain field ($R = R_b$) and centered at a range r_c and azimuth angle θ_c from the radar. Further, the rain rate within the cell has an axisymmetric Gaussian distribution. The parameter L characterizes the width of the cell at the half-peak rain-rate level.

Throughout the paper point (intrinsic) values of radar variables are used; these correspond to infinitesimal resolution volume and will be designated with a subscript i. For a given spatial distribution of rain rate R, the point values of the radar reflectivity factor Z_i, the total differential phase Φ_{DPi}, and the specific differential phase K_{DPi} can be computed using the Marshall–Palmer $R(Z_i)$ relation and the $R(K_{DPi})$ relation

$$R = 40.6|K_{DP}|^{0.866}\ \mathrm{sign}(K_{DP}), \tag{1}$$

specified by Sachidananda and Zrnic (1987) and Ryzhkov and Zrnic (1996). This relation is used to eliminate biases caused by noise at low rain rates. The total differential phase $\Phi_{DPi}(r, \theta)$, along a ray in the azimuthal direction θ is given by the integral

$$\Phi_{DPi}(r, \theta) = \Phi_{DPi}(r_0, \theta) + 2\int_{r_0}^{r} K_{DPi}(x, \theta)\, dx, \tag{2}$$

where r_0 is a reference range anywhere between the radar and the cell.

It is convenient to model Φ_{DPi} at the reference distance r_0 with a linear function of θ,

$$\Phi_{DPi}(r_0, \theta) = \Phi_{0i} + \beta(\theta - \theta_c). \tag{3}$$

This is a simplified representation of azimuthal nonuniformities in the rain field within the beam between the radar and the reference distance r_0. Nonetheless, it will be shown that this approximation captures the essential characteristics of observations.

The radar measured differential phase Φ_{DP} is different from the intrinsic Φ_{DPi} defined by (2). It is weighted by the radar illumination function $I(\theta, \theta_0)$ (Doviak and Zrnic 1993) as follows (Zrnic and Ryzhkov 1996):

$$\Phi_{DP}(r, \theta) = \arg\int Z_{hvi}(r, \theta) I(\theta, \theta_0)\, \exp[j\Phi_{DPi}(r, \theta)]\, d\theta, \tag{4}$$

where θ_0 is the azimuthal direction of the beam center, and Z_{hvi} is the ''cross'' reflectivity; it is proportional to the product of sample amplitudes at horizontal and vertical polarizations and approximately equal to the geometric mean of Z_{hi} and Z_{vi}. To examine the effects on Φ_{DP}, the difference between Z_{hvi} and Z_{hi} or Z_{vi} is not important, rather it is the spatial change of these variables that matters. Therefore, in (4) Z_{hvi} is replaced with Z_i, which is computed from the spatial distribution of the rain rate R. The Φ_{DPi} is calculated from (2), and implicit in $I(\theta, \theta_0)$ are the assumptions that there is no elevation dependence and that the range extent of the weighting is infinitesimal (i.e., much smaller than the azimuthal extent). Consistent with these caveats, $I(\theta, \theta_0)$ is approximated with a Gaussian function two-way antenna pattern and we assume the one-way 3-dB antenna pattern width to be equal to 1°.

The measured K_{DP} is computed from Φ_{DP} using a least squares fit technique with $N = 16$ as the number of range samples in the fit and a range gate spacing of $\Delta = 0.24$ km. These parameters are normally used for estimating the specific differential phase in convective cells (Ryzhkov and Zrnic 1996). After converting K_{DP} to rain rates (1), we obtain the rain field $R(K_{DP})$. The measured reflectivity factor Z is calculated as

$$Z(r, \theta_0) = \int Z_i(r, \theta) I(\theta, \theta_0)\, d\theta, \tag{5}$$

and the corresponding rain field $R(Z)$ is obtained using the Marshall–Palmer relation. Finally, we compare the original rain-rate field R with $R(Z)$ and $R(K_{DP})$.

In our computations we use the following values of parameters: $R_p = 100$ mm h^{-1}, $R_b = 1$ mm h^{-1}, $r_c = 150$ km, and $L = 3$ km. If the center of the rain cell coincides with the beam center, then the radial rain-rate profiles R, $R(Z)$, and $R(K_{DP})$ do not differ much in shape even at a distance of 150 km from the radar (Fig. 2a). But, if the cell is situated at the periphery of the beam (0.85° off the beam axis), the $R(K_{DP})$ signature dramatically changes (Fig. 2b). Negative K_{DP}'s and, as a result, ''negative'' rain rates appear at the far side of the cell. Note that a negative K_{DP} signature at the rear side of the cell is accompanied by overestimation of

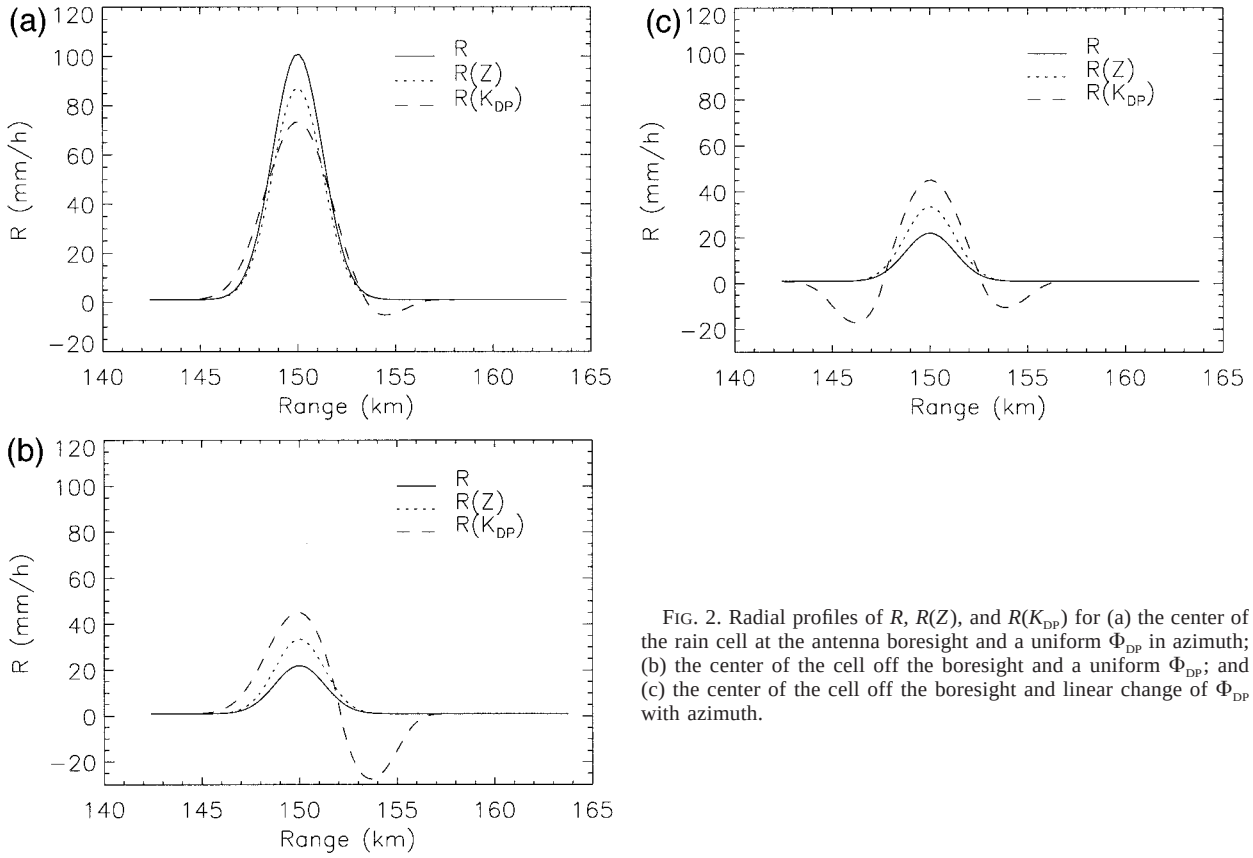

FIG. 2. Radial profiles of R, $R(Z)$, and $R(K_{DP})$ for (a) the center of the rain cell at the antenna boresight and a uniform Φ_{DP} in azimuth; (b) the center of the cell off the boresight and a uniform Φ_{DP}; and (c) the center of the cell off the boresight and linear change of Φ_{DP} with azimuth.

rain rate at the center, that is, positive and negative deviations in $R(K_{DP})$ are coupled.

This finding has important ramification for rain-rate measurements and calls for reexamination of equation (1).

In the examples (Figs. 2a,b) it is assumed that the initial azimuthal distribution of Φ_{DPi} at the reference distance r_0 is uniform; that is, the parameter β in (2) is set to zero. Azimuthal gradients of Φ_{DPi} produce even more peculiar $R(K_{DP})$ signatures. Figure 2c shows that negative K_{DP}'s can appear not only on the rear side of the cell but on its front side too if $\beta \neq 0$. For the situation in Fig. 2c the differential phase gradient β is 10° per 1° of azimuthal change, which is a realistic value in convective storms.

It is instructive to compare two-dimensional images of the rain cell in terms of rain rate obtained using $R(Z)$ and $R(K_{DP})$ relations with the original image (Fig. 3). The same values of parameters R_p, R_b, r_c, and L as in Fig. 2 were used to generate images in Fig. 3. Figure 3b shows a moderate smearing effect on $R(Z)$ in the azimuthal direction (along Y axis), whereas the $R(K_{DP})$ image extends more in azimuth and possesses two negative rain-rate dips at the far side of the cell (Fig. 3c). The $R(K_{DP})$ image is azimuthally symmetric in relation to the center of the cell if the Φ_{DPi} is initially uniform ($\beta = 0$). For $\beta = 10°$ per degree, the $R(K_{DP})$ image becomes more complex with two negative dips of unequal depth; one at the near and the other at the far side of the cell (Fig. 3d). The resulting image is substantially different from the original axisymmetric distribution of rain (Fig. 3a) and shows more spread in both radial and azimuthal directions. Thus, in the presence of large azimuthal changes of Z_i and Φ_{DPi} within the radar sampling volume, the conventional $R(Z)$ estimator more accurately reproduces the actual contours of the remote rain cell than the estimator based on K_{DP}.

In spite of the substantially different shape of the $R(K_{DP})$ image from the original rain field, the integrated rainfall over the area encompassing the rain cell matches the actual areal rainfall (1243 mm h^{-1} km^2, in this particular example) very well. The difference between the actual and estimated areal integrals in Figs. 3b,c is only 4% and 5%, respectively. In other words, positive and negative excursions of K_{DP} [or $R(K_{DP})$] balance each other in the integral sum. This is a very important property of the differential phase estimator of rainfall. Any disturbance of a uniform rain field, such as an isolated rain cell, causes local perturbation in Φ_{DPi} and K_{DPi}. In the case of pronounced nonuniformity within the beam, these perturbations lead to incorrect pointwise estimates of rain rate. At the same time the areal polarimetric estimate of rainfall is practically unbiased, provided that the area boundaries are sufficiently far from the center

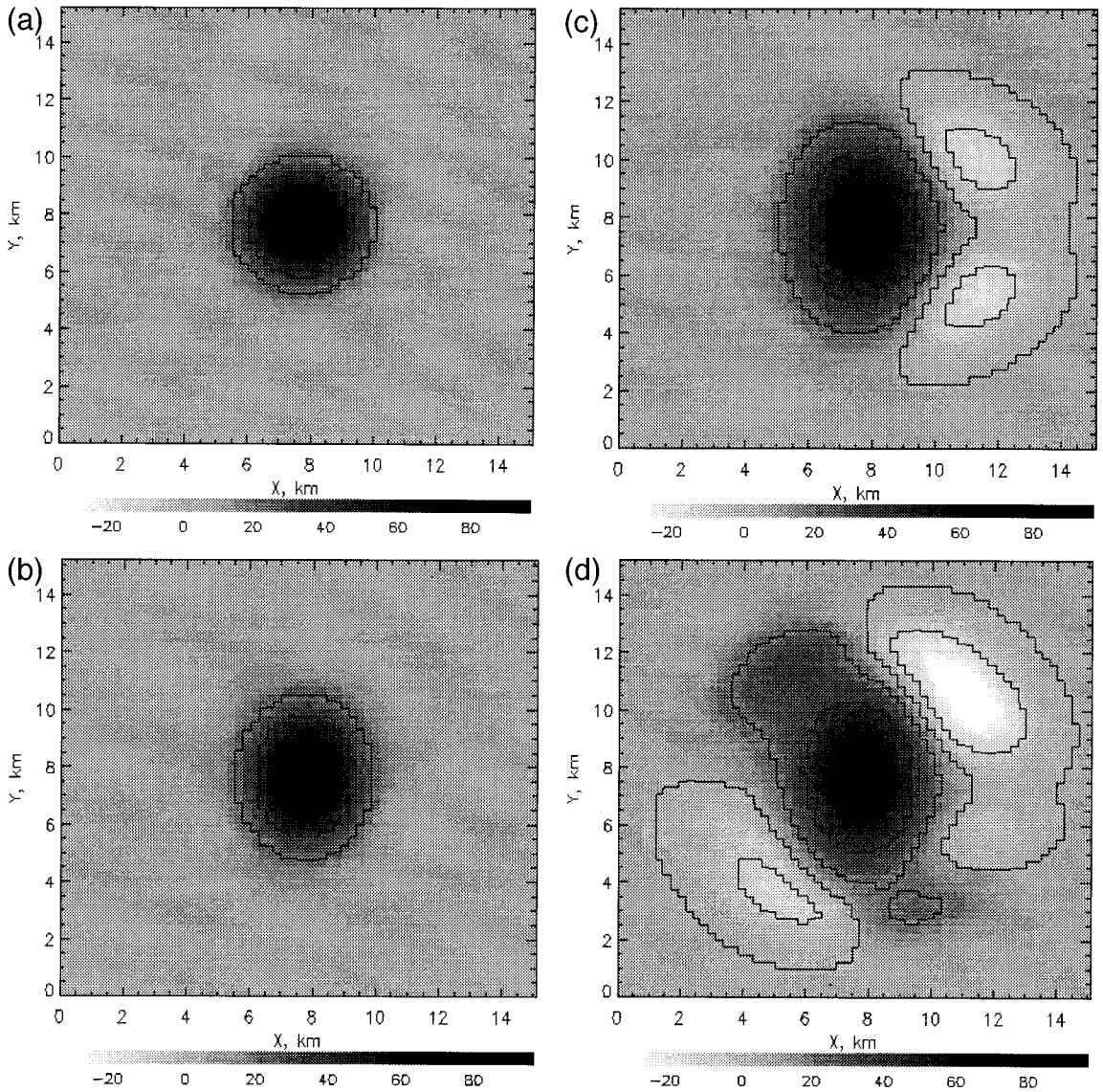

FIG. 3. Two-dimensional images of a rain cell. (a) Actual rain rate R, (b) $R(Z)$, (c) $R(K_{DP})$ for constant initial Φ_{DP} in azimuth, and (d) $R(K_{DP})$ for a linearly changing Φ_{DP} in azimuth. Contours of rain rate are drawn every 20 mm h^{-1}, starting from -20 mm h^{-1}. The radar is located 150 km to the left of the cell.

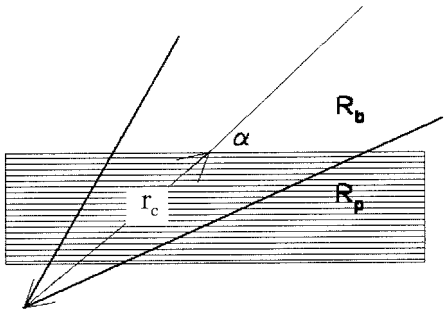

FIG. 4. Conceptual model of a squall line.

of the disturbance. This is consistent with the notion that the path-averaged rain rate depends on the total differential phase along the path. Therefore, the total rainfall is determined by the values of differential phase at the boundaries of the rainy area.

3. Squall line

Next we consider a sharp boundary line, in the rain field, that approximates a leading or trailing edge of a squall line (Fig. 4). It is assumed that the rain rate changes from a large value of R_p to a substantially lower background value R_b across the line. The radar beam is pointing at an angle α with respect to the line. In our

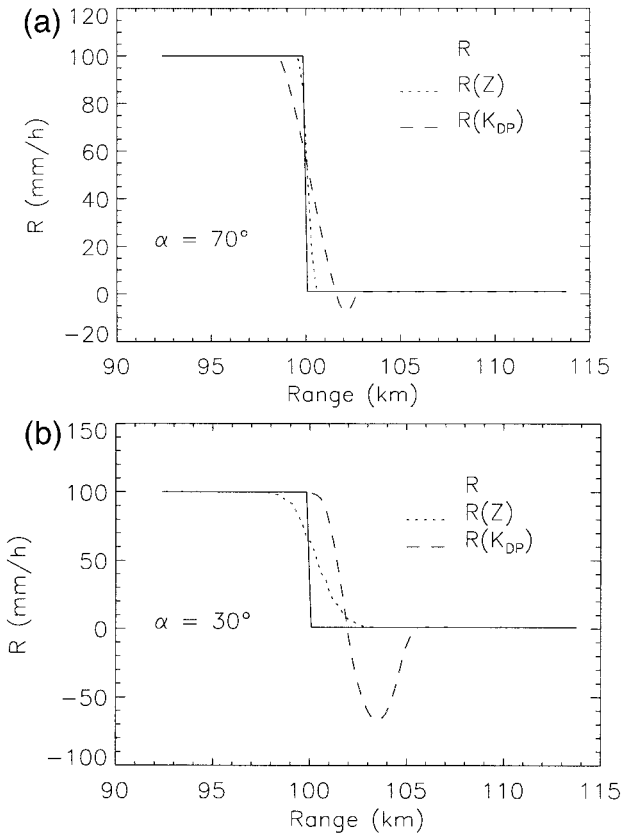

FIG. 5. Radial profiles of R, $R(Z)$, and $R(K_{DP})$ through a squall line for (a) $\alpha = 70°$ and (b) $\alpha = 30°$.

computations $R_p = 100$ mm h^{-1}, $R_b = 1$ mm h^{-1}, and $r_c = 100$ km. It is obvious that the azimuthal change of rain rate (or reflectivity) within the beam depends on the angle α and the range r_c of the crossing point between the line and antenna beam. Therefore, the simulated $R(Z)$ and $R(K_{DP})$ signatures are different for different angles α (Fig. 5). At $\alpha = 70°$ the radial profiles of measured rain rates have minor distortions, and presence of negative K_{DP} [or $R(K_{DP})$] is evident in the low rain-rate region close to the discontinuity (Fig. 5a). The distortions are larger at the angle $\alpha = 30°$. Of the two rain rates, $R(Z)$ better represents the position of the discontinuity. The discontinuity in the $R(K_{DP})$ profile is shifted, and it crosses into a negative rain rate, creating a deep minimum (Fig. 5b). Nevertheless, similarly to the previous case of an isolated cell, the integral sum of precipitation within the interval between 100 and 105 km, computed from $R(K_{DP})$, is very small and contributes little to the areal accumulation.

4. Experimental evidence

Experimental data collected with the Cimarron polarimetric radar indicate that K_{DP} at far distances from the radar sometimes exhibits spurious oscillatory behavior. This seems to occur in the growth stage of isolated convective cells (small sizes compared to the beamwidth) or along the edges of squall lines. The example in Fig. 6 represents the case where strong azimuthal gradients of Z and Φ_{DP} are evident in the area where the squall line stretches almost along the radar beam. Radial dependence of Φ_{DP} taken at the azimuthal direction 63.6°, indicated as a white line in Fig. 6, is definitely affected by the gradients within the beam (Fig. 7a). The large fluctuations (180°) near 110 km and a spike at 160 km in the unprocessed Φ_{DP} data are caused by aliasing at the phase transition boundaries (−80° and 100° for the Cimarron radar). These data are dealiased by examining continuity in range and are smoothed with a running average over about 7.7 km (32 consecutive samples). The corresponding profiles of rain rate derived from Z and K_{DP} are shown in Fig. 7b. For the cells centered at the distances of 36 and 107 km, the $R(K_{DP})$ signature is similar to that shown in Fig. 2b. At the center of these cells the $R(K_{DP})$ relation gives a larger rain rate than the $R(Z)$ relation, whereas at the far side of the cells the $R(K_{DP})$ yields negative rain rates. At distances over 130 km, $R(Z)$ and $R(K_{DP})$ are uncorrelated. The large oscillations (wavelength of about 14 km) of Φ_{DP} and $R(K_{DP})$ are attributed to nonuniform beamfilling. Statistical noise causes the rapid fluctuations of Φ_{DP} on scales of the range gate spacings.

As stated in section 2 negative K_{DP} can appear on both sides of isolated rain cells if the initial azimuthal distribution of Φ_{DP} is not uniform (see Fig. 2c). To substantiate this point, an example of real data is represented in Fig. 8. The data were collected with the NCAR S-POL (10-cm wavelength) polarimetric radar in Colorado on 17 July 1996. The strong isolated convective cell exhibits a well-pronounced hail signature in terms of the maximum reflectivity that exceeds 60 dBZ and differential reflectivity Z_{DR} that is close to zero in the core. Here, K_{DP} has a negative minimum in front of and behind the cell. These negative excursions of K_{DP} could not be caused by backscatter differential phase because they are observed in the zones of quite low reflectivity (below 40 dBZ) where the Mie effects are unlikely. A feasible explanation of negative K_{DP}'s is nonuniform beamfilling, considering the extreme strength and small size of this hail-bearing cell. This finding raises questions about interpretations of differential phase in hailstorms (Zrnic et al. 1993a), where nonmonotonic range dependence of Φ_{DP} within a strong convective core was attributed to a backscatter differential phase.

A natural concern is the percentage of contaminated data in the radar image of a typical convective system. Since large negative K_{DP} is a manifestation of an artifact (apart from backscatter differential phase and vertically aligned crystals in the presence of strong electric fields), the total area where K_{DP} is below a certain negative value divided by the total rainy area can serve as a measure of contamination. The negative threshold for K_{DP} must have a large enough magnitude to filter out ''normal'' statistical fluctuations of the K_{DP} estimate in low re-

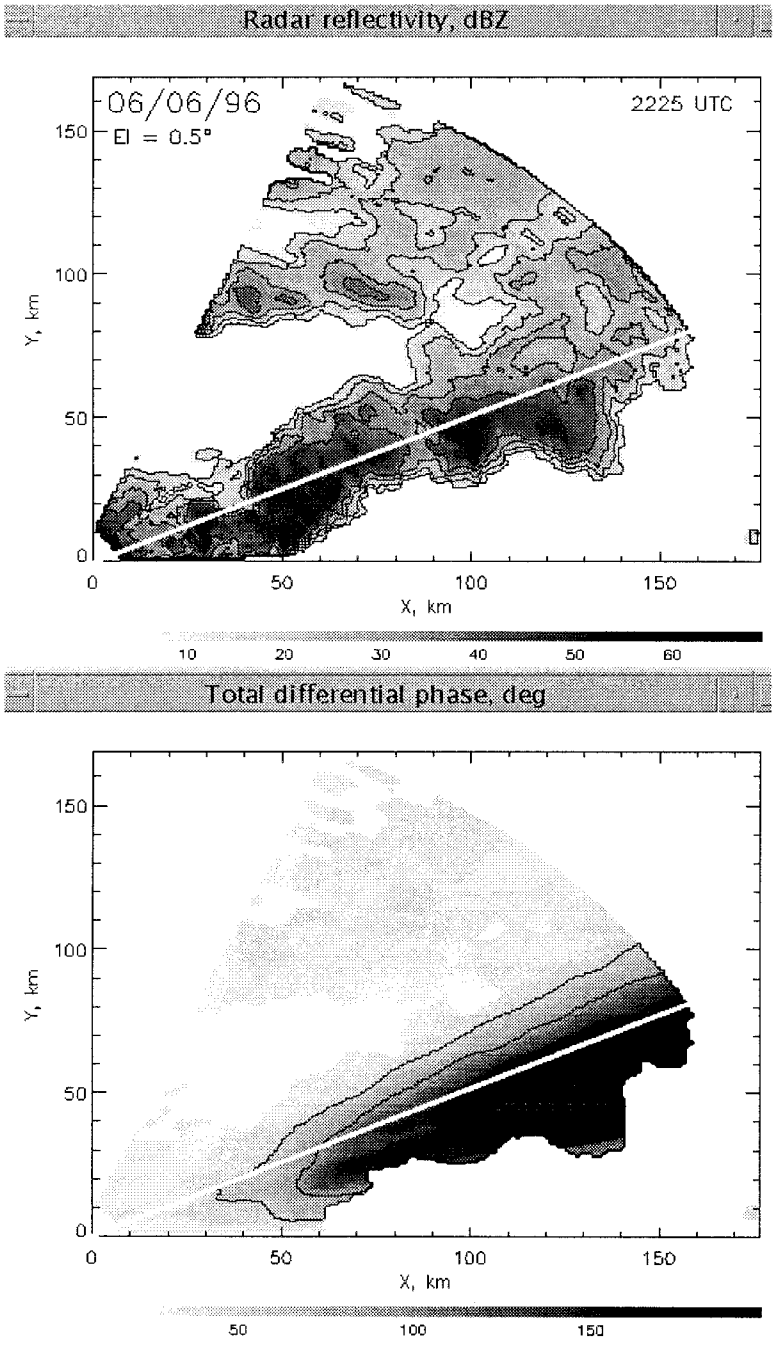

FIG. 6. Sector PPI images of Z and Φ_{DP} in the case with pronounced azimuthal gradients. The contours of Z are drawn 10 dBZ apart, starting at 10 dBZ and the contours of Φ_{DP} are at 50° intervals, starting from 50°. The time is 2225 UTC 6 June 1996 and the elevation is 0.5°. The white line shows the azimuth of 63.6°.

flectivity areas. If the number of successive Φ_{DP} samples in the range resolution interval for K_{DP} estimation is set to 16, then the standard deviation of the K_{DP} estimate is about 0.3°–0.5° km^{-1} (Ryzhkov and Zrnic 1996). This means that by selecting the threshold within the interval between $-1.0°$ and $-1.5°$ km^{-1} we can filter out 99% of random fluctuations of K_{DP} in low reflectivity regions.

We examined three cases of squall lines consisting of clusters of more or less isolated convective cells. These occurred on 9 June 1993, 6 May 1995, and 6 June 1996. At the elevations of 0.5° the number of range locations where K_{DP} is less than -1.0 (or $-1.5°$ km^{-1}) was determined and divided by the total number of locations where the radar reflectivity factor is over 12 dBZ. The

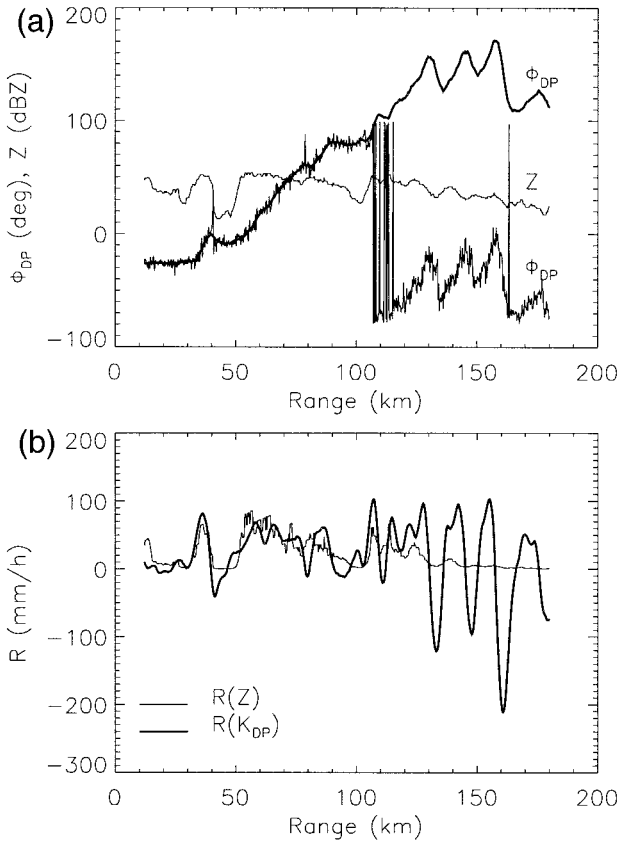

FIG. 7. Radial profiles of (a) Z, Φ_{DP} and (b) $R(Z)$, $R(K_{DP})$. The time is 2225 UTC 6 June 1996, the elevation is 0.5°, and the azimuth is 63.6°.

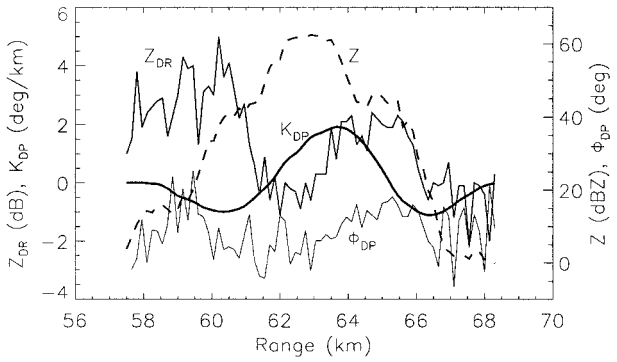

FIG. 8. Radial profiles of Z, Z_{DP}, K_{DP}, and Φ_{DP} through an isolated hailstorm that occurred on 13 July 1996 in Colorado and was observed with the NCAR's polarimetric radar. The elevation is 0.5°, the azimuth is 302.6°, and the time is 2105 UTC.

radar coverage area for all cases extended to 180 km in range. Table 1 lists the average fractions for each storm at the K_{DP} thresholds of $-1.0°$ and $-1.5°$ km^{-1}. In the worst case of the storm of 6 June 1996 the fraction of negative K_{DP}'s below the threshold of $-1.0°$ km^{-1} is relatively small and does not exceed 1.5%.

5. Melting layer

A common situation of nonuniform beamfilling occurs when the horizontal melting layer of stratiform clouds is observed at low elevation angles. In such cases the nonuniformity is in the elevation direction rather than the azimuthal direction. The smoothing effect of antenna beam leads to a reduction of the peak radar reflectivity and differential reflectivity within the bright band. Another consequence is a wavelike Φ_{DP} in the radial profile of total differential phase at the distances where radar beam crosses the melting layer. Such a signature was first reported by Zrnic et al. (1993b), who associated it with the backscatter differential phase. A positive Φ_{DP} half-wave was attributed to the aggregates with sizes between 10 and 14 mm, while the negative half-wave was associated with smaller aggregates in the 8–10-mm size range. Although we do not have evidence to refute the interpretation in Zrnic et al. (1993b), we offer an alternative interpretation that is based on the model of nonuniform beamfilling. According to the Ockham's razor principle (Jeffreys and Berger 1992), this interpretation might be more likely because it is simpler. The principle implies that ''an explanation of facts should be no more complicated than necessary'' or that ''among competing hypotheses, favor the simplest one.'' Under some circumstances the Ockham's razor is a consequence of a deeper law tied to the Bayesian statistical analysis.

To simulate differential phase within the melting layer using the method described in section 1, realistic assumptions about vertical profiles of Z and K_{DP} should be made. The vertical structure of Z within the melting layer is well known (see Battan 1970; or Fabry and Zawadzki 1995, for example). Much less information about the vertical profiles of polarimetric variables, especially K_{DP}, is available. It was established that the maximum of differential reflectivity Z_{DR} is usually located in the lower part of the melting layer below the peak of radar reflectivity factor Z (Moninger et al. 1984; Zrnic et al. 1993b; Russchenberg and Lighthart 1996). Our measurements in snow (Ryzhkov and Zrnic 1998) show that both Z_{DR} and K_{DP} are quite low if the snow comprises large low-density aggregates. The examination of radar polarimetric variables across the frontal boundary between snow and rain near the ground indicates that Z_{DR} and K_{DP} reach their maxima in the transition zone almost simultaneously, and even in this zone K_{DP} is still below 0.2°–0.3° km^{-1} at the 10-cm wave-

TABLE 1. The average fraction of contaminated areas for three Oklahoma storms.

K_{DP} threshold (deg km^{-1})	9 June 1993	6 May 1995	6 June 1996
−1.0	0.69%	1.05%	1.45%
−1.5	0.20%	0.43%	0.63%

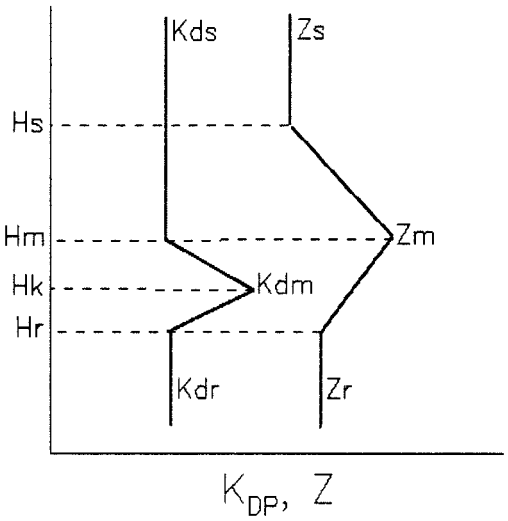

FIG. 9. Conceptual model of vertical profiles of Z and K_{DP} within the melting layer.

length (Ryzhkov and Zrnic 1998). From these considerations we submit in Fig. 9 the conceptual model of vertical dependencies of Z and K_{DP}.

To make comparison between real data and simulation we chose the 4 June 1995 case and present vertical cross sections of pertinent variables in Fig. 10. Clearly, in the stratiform precipitation between two convective lines (40–70 km from the radar) a pronounced bright band is visible in the Z and K_{DP} fields. Two adjacent horizontal slabs of enhanced positive and negative K_{DP} mark the melting layer at the height of approximately 3 km above the ground. Another zone of negative K_{DP} exists at the height interval between 6.5 and 8.5 km and ranges from 80 to 100 km. This is a region of ''true'' negative K_{DP} caused by the presence of vertically oriented crystals. It has been observed in other locations (Caylor and Chandrasekar 1996) and explained as a consequence of strong vertical electric fields in the top region of updraft that orient elongated crystals in the direction of field lines.

We have selected a profile of the total differential phase at the elevation angle of 3.0° (Fig. 11). Twenty radials of Φ_{DP} data from consecutive azimuths (about 20°) were averaged to produce the graphs in Fig. 11. The average radial profile of Φ_{DP} is depicted as a dashed line in Fig. 11a. The range derivative of this profile produces the K_{DP} oscillation seen in the melting layer (Fig. 10).

Next we simulate the observed radial profile of Φ_{DP} using the conceptual model of the melting layer (Fig. 9) and a realistic combination of parameters characterizing vertical profiles of Z and K_{DP} as well as realistic distribution of initial elevation dependence of Φ_{DP} at a reference range r_0 from the radar. In our analysis we set $r_0 = 35$ km and determined, from the data, that $\Phi_{DP}(r_0)$ increases with increasing elevation angle at a rate $\beta =$ 7°–8° per degree. As a first step the simulated vertical profile of radar reflectivity factor is matched to the observed. Figure 12 shows that the model vertical profile of Z (with parameters Zm = 43 dBZ, Zr = 27 dBZ, Zs = 20 dBZ, Hr = 3.0 km, Hm = 3.2 km, and Hs = 3.3 km) is a good approximation of the measured vertical profile at least in the height interval between 2.5 and 3.5 km above ground. In the simulation of the measured Z, weighting by the radar antenna pattern with the beamwidth of 0.9° has been applied. The measured vertical profile of Z is the average of individual vertical profiles in the range interval between 40 and 50 km from the radar (see Fig. 10). Note that the measured vertical profile of Z is quite different from the actual one (not weighted by the antenna pattern). The maximum value of Z is negatively biased by almost 10 dB, and the peak of Z is displaced by 300 m in height.

The simulated K_{DP} below and above the melting layer is selected to be consistent with the corresponding reflectivity values. That is, in rain the Kdr and Z are related via the Marshall–Palmer relation (Fig. 8.25 in Doviak and Zrnic 1993), thus Kdr = 0.02° km^{-1}. In snow Kds is also set to 0.02° km^{-1}, which is consistent with previous observations (Ryzhkov and Zrnic 1998). Neither of these two values has much influence on the measured profile K_{DP}, but the peak value of K_{DP} does. By trial and error we found that $K_{dm} = 0.4°$ km^{-1} at the height Hk = 3.1 km matches the observations well. The underlying (within the beam) gradient of Φ_{DP} was obtained by extrapolating measurements from elevations below the melting layer, thus $\beta = 7°$ per degree.

The simulated radial profile of differential phase is shown by a solid line in Fig. 11a. Simulated and observed profiles of Φ_{DP} agree fairly well, considering the simplicity of the melting layer model. This example shows that it is possible to explain the observed behavior of differential phase in the melting layer within a framework of the model of nonuniform beamfilling without resorting to the Mie effects. It is important to note that the shape of the differential phase radial profile through the melting layer depends crucially on the angular (elevation) distribution of Φ_{DP} at ranges ahead of the melting layer. A change of β dramatically affects the shape of the Φ_{DP} profile. Figure 11b illustrates the profile for which $\beta = 0$. The wavelike signature completely disappears. This type of ''plain'' Φ_{DP} profile was observed at some azimuthal directions in the stratiform part of the same 4 June 1995 storm. In other words, both the transverse Z and Φ_{DP} gradients substantially affect the profile of differential phase along a radial if a strong nonuniformity exists within the beam.

6. Discussion

Along with several important advantages (listed in section 1) inherent to measuring precipitation by using a specific differential phase, there are two shortcomings compared to the traditional $R(Z)$ algorithm. First, it pro-

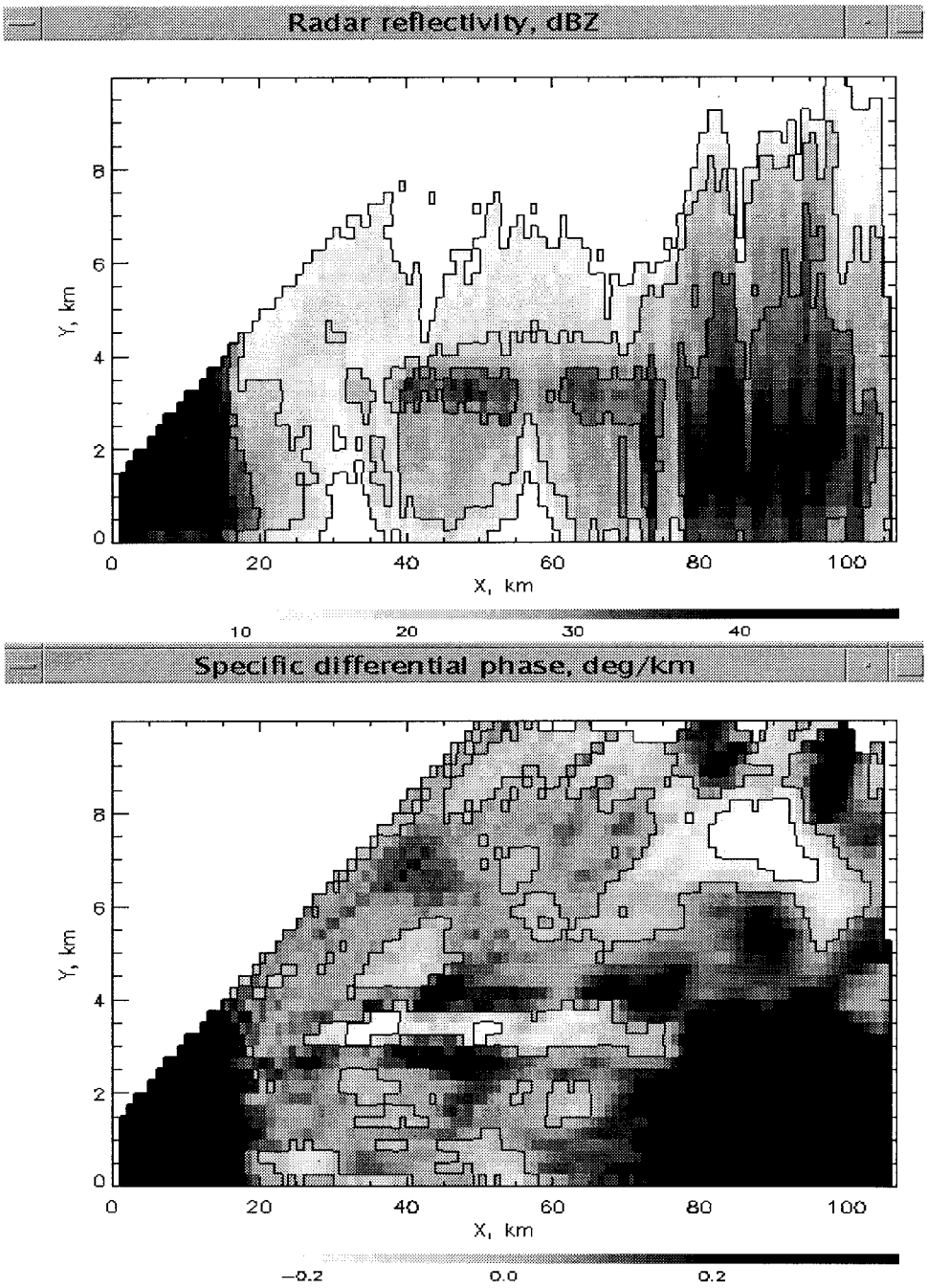

FIG. 10. Vertical cross sections of Z and K_{DP} for the storm on 4 June 1995. The azimuth is 325°. The contours of Z are drawn 10 dBZ apart starting at 10 dBZ, and the contours of K_{DP} are at 0.2° km^{-1} intervals starting from −0.2° km^{-1}. Between 40 and 70 km is a well-defined melting layer.

vides worse spatial resolution of rainfall estimates, and second, it is more affected by nonuniform beamfilling.

The first disadvantage has a relatively minor consequence. The actual radial resolution of 2–4 km achievable in convective situations (given 16 consecutive gates of an averaging window for the K_{DP} estimate) is close to the resolution requirement (2 km × 2 km) accepted by the operational community. In stratiform rain with reflectivities lower than 40 dBZ a three times larger averaging scale is recommended for the K_{DP} estimate (Ryzhkov and Zrnic 1996). In spite of the fact that pointwise instantaneous polarimetric estimates of low rain rates have large standard errors, the corresponding rain accumulation over sufficiently large areas (sizes of about 10 km) are quite reliable. They are better than those made using the $R(Z)$ algorithm that suffers from

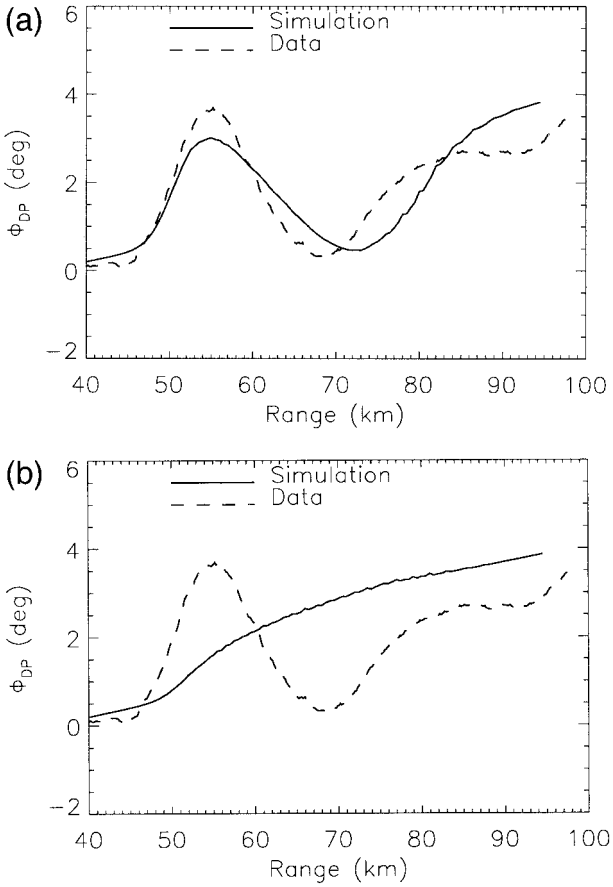

FIG. 11. Radial profiles of Φ_{DP} within the melting layer inferred from the data and simulation. (a) Actual linear dependence of Φ_{DP} in elevation is modeled. (b) A uniform Φ_{DP} is assumed. Elevation is 3.0°.

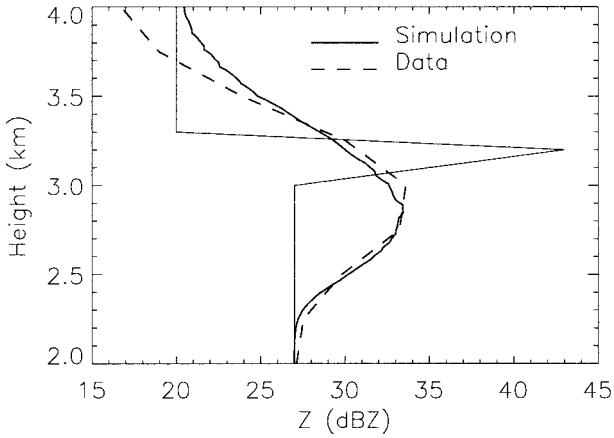

FIG. 12. Vertical profiles of Z measured by the radar and simulated. The thin solid line is a perfectly resolved profile of Z (not smoothed by radar beam).

radar miscalibration, attenuation, drop size distribution uncertainties, partial beam blockage, and presence of hail (Ryzhkov and Zrnic 1996). Thus, some degradation of spatial resolution is tolerable, keeping in mind other indisputable advantages of the polarimetric method.

The second problem poses a more serious threat to the accuracy of polarimetric rainfall estimation, especially at large distances from the radar. The examples given in this paper indicate that polarimetric point estimates of rain rate might be completely erroneous if the azimuthal changes of Z and Φ_{DP} within the radar resolution volume are sufficiently large. These contaminated regions are easy to recognize from large negative values of K_{DP}. Most often the areas of negative K_{DP} appear at the periphery of intense convective cells where the actual rainfall is low. Nonetheless, it would be wrong to ignore or discard these negative K_{DP}'s because they are always coupled with positively biased K_{DP} nearby at the center of the cell. One way to deal with this problem is by combining the advantages of both methods—$R(Z)$ and $R(K_{DP})$. For example, capitalize on the fact that, as shown in sections 2 and 3, the radial integral of $R(K_{DP})$ over the interval containing both negative and positive peaks of K_{DP} is an almost unbiased estimate of the true integral sum. Therefore, in the area of contamination, apply the conventional $R(Z)$ algorithm to retrieve radial profile of rain rate, then unbias it using the areal integral computed from $R(K_{DP})$. A similar idea of using a Z–K_{DP} scattergram to get a polarimetrically tuned $R(Z)$ relation was expressed by Ryzhkov et al. (1997). In this manner such advantages of the $R(Z)$ method as fine spatial resolution and better immunity to the nonuniform beamfilling are combined with the $R(K_{DP})$ method's advantages.

7. Conclusions

We have examined the effects of nonuniform radar beamfilling on the performance of the rainfall estimator that uses the specific differential phase K_{DP}. Two simple models of nonuniform beamfilling were considered: an isolated rain cell with azimuthal size comparable to the beamwidth and a line of sharp reflectivity change seen at an angle from the radar.

The polarimetric estimator $R(K_{DP})$ distorts the shape of the isolated cell more than the conventional $R(Z)$ algorithm. These distortions are manifested as negative K_{DP}'s at the periphery of the rain cell. The exact location of the regions of negative K_{DP} crucially depends on the azimuthal gradient of total differential phase within the radar resolution volume. In the case of a squall line that is moving away from the radar, the apparent leading edge is shifted ahead of the line and is preceded by areas of negative K_{DP}'s. The distortion increases with the decreasing angle between the squall line and the radar beam. However, in both cases the integral of $R(K_{DP})$ along the radial encompassing the distortions yields a reasonably accurate estimate of the actual integrated rainfall.

Experimental data collected with the Cimarron polarimetric radar confirm the results of theoretical sim-

ulations. The contamination of polarimetric rainfall estimates by the nonuniform beamfilling effects is most pronounced at large distances from the radar. It requires the presence of strong isolated convection or squall lines consisting of discernible cells. Overall, this artifact was observed in less than 1.5% of the total radar coverage area containing precipitation. The radar coverage in these observations was 180 km.

To improve the quality of rain estimates in the contaminated areas we recommend that the rain-rate distribution be retrieved first with an $R(Z)$ algorithm. Then this distribution should be adjusted using the unbiased polarimetric estimate of the areal rainfall integral as a calibration constant.

Angular gradients of Z and total differential phase Φ_{DP} in the elevation direction might be responsible for the wavelike Φ_{DP} signature previously observed at the distances where the radar beam intersects the melting layer of stratiform precipitation. We have presented an alternative explanation of the observed signature that differs from the one based on the Mie effects and backscatter differential phase. Although we have no evidence to refute the previous explanation, the current model is favored because of its simplicity.

Acknowledgments. We are grateful to Ed Brandes for providing polarimetric data collected with the NCAR S-POL radar from which Fig. 8 was generated. Mike Schmidt and Richard Wahkinney have maintained and calibrated the Cimarron radar. This research was partly supported by the National Weather Service's Office of Hydrology.

REFERENCES

Battan, L. J., 1973: *Radar Observations of the Atmosphere.* University of Chicago Press, 323 pp.

Caylor, J., and V. Chandrasekar, 1996: Time-varying ice crystal orientation in thunderstorms observed with multiparameter radar. *IEEE Trans. Geosci. Remote Sens.,* **34,** 847–858.

Doviak, R. J., and D. S. Zrnic, 1993: *Doppler Radar and Weather Observations.* Academic Press, 562 pp.

Fabry, F., and I. Zawadzki, 1995: Long-term radar observations of the melting layer of precipitation and their interpretation. *J. Atmos. Sci.,* **52,** 838–851.

Jefferys, W. H., and J. O. Berger, 1992: Ockham's razor and Bayesian analysis. *Amer. Sci.,* **80,** 64–72.

Moninger, W. R., V. N. Bringi, T. R. Detman, J. R. Jordan, T. A. Seliga, and K. Aydin, 1984: Melting layer observations during MAYPOLE. Preprints, *22d Conf. on Radar Meteorology,* Zurich, Switzerland, Amer. Meteor. Soc., 364–369.

Russchenberg, H. W. J., and L. P. Lighthart, 1996: Backscattering by and propagation through the melting layer of precipitation: A new polarimetric model. *IEEE Trans. Geosci. Remote Sens.,* **34,** 3–14.

Ryzhkov, A. V., and D. S. Zrnic, 1996: Assessment of rainfall measurement that uses specific differential phase. *J. Appl. Meteor.,* **35,** 2080–2090.

——, and ——, 1998: Discrimination between rain and snow with a polarimetric radar. *J. Appl. Meteor.,* in press.

——, ——, and D. Atlas, 1997: Polarimetrically tuned $R(Z)$ relations and comparison of radar rainfall methods. *J. Appl. Meteor.,* **36,** 340–349.

Sachidananda, M., and D. S. Zrnic, 1987: Rain-rate estimates from differential polarization measurements. *J. Atmos. Oceanic Technol.,* **4,** 587–598.

Zrnic, D. S., and A. V. Ryzhkov, 1996: Advantages of rain measurements using specific differential phase. *J. Atmos. Oceanic Technol.,* **13,** 454–464.

——, V. N. Bringi, N. Balakrishnan, K. Aydin, V. Chandrasekar, and J. Hubbert, 1993a: Polarimetric measurements in a severe hailstorm. *Mon. Wea. Rev.,* **121,** 2223–2238.

——, N. Balakrishnan, C. L. Ziegler, V. N. Bringi, K. Aydin, and T. Matejka, 1993b: Polarimetric signatures in the stratiform region of a mesoscale convective system. *J. Appl. Meteor.,* **32,** 678–693.